

Standing Helicon Wave Induced by a Rapidly Bent Magnetic Field in Plasmas

Kazunori Takahashi,^{*} Sho Takayama, Atsushi Komuro, and Akira Ando
Department of Electrical Engineering, Tohoku University, Sendai 980-8579, Japan
(Received 8 February 2016; published 30 March 2016)

An electron energy probability function and a rf magnetic field are measured in a rf hydrogen helicon source, where axial and transverse static magnetic fields are applied to the source by solenoids and to the diffusion chamber by filter magnets, respectively. It is demonstrated that the helicon wave is reflected by the rapidly bent magnetic field and the resultant standing wave heats the electrons between the source and the magnetic filter, while the electron cooling effect by the magnetic filter is maintained. It is interpreted that the standing wave is generated by the presence of a spatially localized change of a refractive index.

DOI: 10.1103/PhysRevLett.116.135001

The helicon wave is one of the fundamental Whistler waves in plasmas [1–3]. The wave fields efficiently heat electrons in plasmas and yield highly ionized plasmas for wide ranges of parameters such as neutral pressure, rf frequency, and magnetic field strength [4–8]. Some aspects of the wave behaviors have been well understood by a wave dispersion theory incorporating boundary conditions of the metallic and/or dielectric walls [2,3], while some experiments have shown the helicon wave in unbounded plasmas [9–11]. Because of the boundary conditions or antenna configurations, a standing helicon wave and the resultant high density plasma are sometimes formed in artificial plasma devices [1,12–15]. The wave propagation and absorption in nonuniform magnetic fields have also already been investigated [8,16]. It is typically assumed that the characteristic length of the variation of the refractive index is much longer than the wavelength, i.e., the Wentzel-Kramers-Brillouin (WKB) approximation [17]. Since the dielectric tensor in cold plasmas depends on the local plasma density and the static magnetic field, the refractive index spatially varies for cases of the nonuniform density and magnetic field. Under the WKB-approximated situation, a ray tracing analysis can provide the trajectory of the wave, where the wave is refracted by the nonuniform refractive index [18]. On the other hand, nonuniform profiles of the dielectric constant with a comparable or shorter scale length than the wavelength have given rise to inherent characteristics of the wave propagation regardless of the presence of the plasmas, e.g., wave mode conversions in plasmas [19,20], and a wave band gap in photonic crystals with no plasma [21,22]. It has also been demonstrated that the periodic structure of the plasma density with a similar scale to the wavelength yields metamaterial characteristics [23]. The situation in which the WKB approximation cannot be applied might sometimes appear in artificial rf plasma devices, e.g., the localized jump of the plasma density due to a current-free double layer [24], and a rf negative hydrogen or deuterium ion source having a magnetic filter (MF) [25,26].

The negative ion source is a key technology of the neutral beam injection (NBI) heating [27–29] in thermonuclear fusion plasmas. The ion sources typically consist of a plasma production region, the MF region having the vertical magnetic field, and beam extraction grids. The negative ions are mainly produced at the first grid (called a plasma grid) contacting to the upstream plasma, via reactive surface processes of the hydrogen or deuterium positive ions and excited atoms with the low work function materials [30,31]. Since the negative ions are destructed by collisions with high energy electrons, an electron temperature has to be reduced near the plasma grid by the MF [26,32]. On the other hand, densities of the positive ions and excited atoms just upstream of the MF are required to be high for the high production rate of the negative ions [25], which can be obtained for a high electron temperature due to collisional processes. Therefore, both the high and low electron temperatures upstream of the MF and near the plasma grid, respectively, have to be maintained for the negative ion source. The rf plasma source is also one of the options for performing a longtime operation of the NBI [25,28]. Combination of the helicon-wave discharge having an axial magnetic field and the MF is also one of the candidates to yield the upstream high density plasma [33,34]. Since the dielectric tensor in plasmas under the magnetic field is anisotropic, the refractive index strongly depends on the magnetic field direction as well as the magnetic field strength and the plasma density; hence, the refractive index under the complex magnetic field is expected to be very nonuniform and to yield unexpected wave characteristics for the non-WKB-approximated configuration.

In this Letter, a localized electron heating due to a standing helicon wave, which originates from the wave reflection by rapid change of the refractive index, is experimentally demonstrated by a combination of the helicon source and the downstream MF, where the scale length of the spatial variation of the refractive index is shorter than the wavelength. By incorporating such a

magnetic field structure, both the electron heating in front of and cooling within the MF are simultaneously demonstrated.

Experiments are performed in the hydrogen helicon source attached to a diffusion chamber [Fig. 1(a)], where the vertical magnetic field called the MF is applied to the diffusion chamber. The helicon source consists of a 70 mm inner diameter and 175 mm long ceramic tube wound by a four-turn $m = 0$ mode loop antenna, where the upstream side of the tube is terminated by a grounded flange ($z = 0$) and m is the azimuthal mode number. Hydrogen gas is introduced from the upstream side and the pressure is maintained at 1 Pa. Two solenoids are centered at $z = 40$ and 140 mm and a dc current of 40 A is supplied to each of the two solenoids to provide the axial magnetic field. The magnetic field strength $B_{z\text{sol}}$ provided by the solenoids on the axis is plotted by a solid line in Fig. 1(b). The axial magnetic field on the z axis is about 15 mT and decreases to about 3.5 at $z = 250$ mm. Two rectangular permanent magnets (PMs) are located outside of the chamber. Figure 1(b) shows the x component of the magnetic field $B_{x\text{PM}}$ provided by only the PMs for the axial locations of the PMs of $z = 250, 230,$ and 222 mm, which are labeled as configurations A–C, respectively. The actual magnetic field is given by a sum of the fields provided by the solenoids and the PMs; the calculated two-dimensional profiles of the local magnetic field strength and the vector for configuration A are shown in Fig. 1(a). The magnetic field

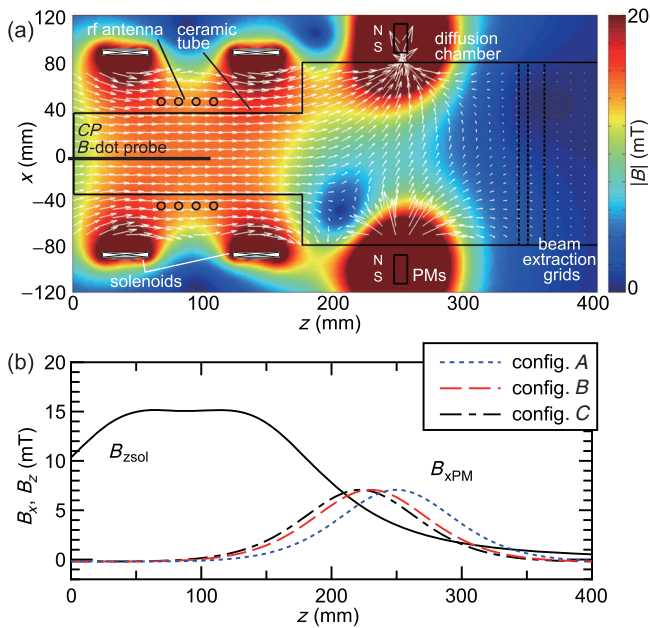


FIG. 1. (a) Schematic diagram of the experimental setup together with the contour plot of the magnetic field strength and arrows showing the local magnetic field vector for configuration A. (b) Axial profiles of the axial magnetic field $B_{z\text{sol}}$ provided by the solenoids and the vertical magnetic field $B_{x\text{PM}}$ provided by the PMs for configurations A–C.

lines are rapidly bent over $z \sim 200$ –250 mm by the presence of the MF. Beam extraction grids are located at $z = 340$ mm and grounded in the present experiments. The rf antenna is powered by an 8 MHz rf amplifier through an impedance matching circuit, and the rf power is maintained at 4 kW.

An axially movable rf-compensated Langmuir probe (CP) is inserted as shown in Fig. 1(a). An electron energy probability function (EEPF) $g_p(\epsilon_e)$ is obtained by an analogue differentiation technique, and ϵ_e is the electron energy [35]. Figures 2(a) and 2(b) show the measured EEPFs along the z axis for configuration A (with the solenoids and the PMs) and the case with no MF (with only the solenoids), respectively. The clear difference between the two cases is seen in the EEPFs taken at $z \sim 220$ mm; it is found that the high temperature electrons exist around $z \sim 220$ mm only for configuration A. On the other hand, the electron temperature at $z \sim 300$ mm for configuration A [Fig. 2(a)] seems to be significantly lower than that for the case with no MF [Fig. 2(b)].

An effective electron temperature T_{eff} is obtained by integrating the measured EEPF [35], while the plasma density n_p is estimated from the ion saturation current. The axial profiles of T_{eff} and n_p on axis are plotted in Figs. 2(c) and 2(d), respectively. For the three configurations (A–C), the localized increase in T_{eff} at $z \sim 200$ –220 mm is seen in Fig. 2(c). Although the plasma density gradually decreases along z inside the source tube ($z < 175$ mm), an increase in the plasma density in the high temperature region ($z \sim 220$ mm) is detected as shown in Fig. 2(d). Therefore, the high density plasma around $z = 220$ mm originates from the ionization process by the high temperature electrons existing there. At $z > 250$ mm, on the other hand, the effective electron temperature is found to decrease along the axis, which seems to be due to the MF effect, as reported previously [26,32]. It should be mentioned that the high electron temperature and high density region downstream of the source moves together with the MF. For the case with no MF, the high temperature electrons and the high plasma density around $z \sim 220$ mm cannot be observed. Hence, it can be deduced that the localized high temperature electrons and high density plasmas downstream of the source arise from the presence of the MF.

To reveal the relation between the electron heating and the rf field, the axial profile of the rf magnetic field is measured. A rf B-dot probe detecting the z component of the magnetic field is inserted instead of the CP. The rf antenna current is simultaneously measured by a Rogowski coil as a phase reference.

Figure 3 shows the axial profiles of the amplitude $|dB/dt|$ of the B-dot probe signal and the phase difference $\Delta\phi$ with respect to the antenna current for the same conditions as in Fig. 2. For all of the cases, $|dB/dt|$ exponentially decays along the axis in the region of

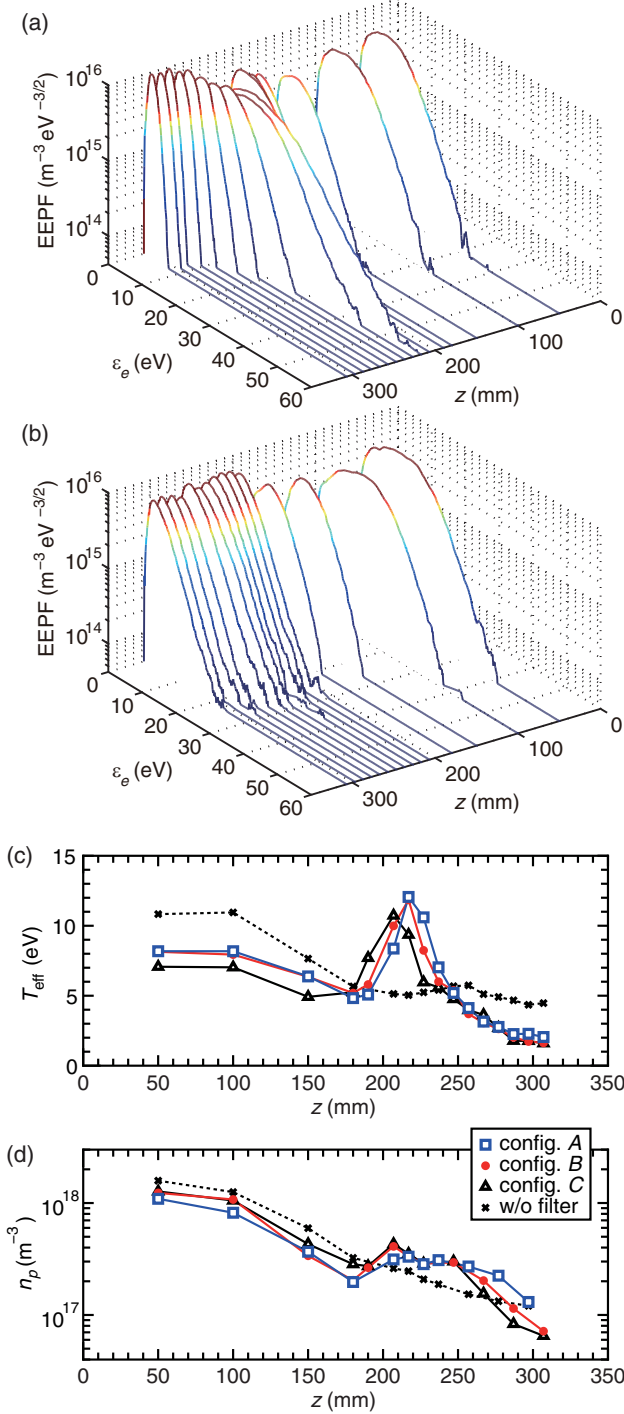


FIG. 2. Measured EEPFs along the z axis for cases (a) of configuration A and (b) with no magnetic filter. (c) Effective electron temperature T_{eff} calculated from the EEPFs measured along the z axis. (d) Plasma density n_p along the z axis. The open squares, filled circles, open triangles, and crosses in Figs. 2(c) and 2(d) are taken for configurations A, B, and C, and with no magnetic filter, respectively.

$z < 175$ mm. For the configurations A–C with the MF, the localized increase in $|dB/dt|$ is detected at $z \sim 175$ – 230 mm; a wave node seems to exist at $z \sim 175$ mm, e.g., clearly seen for configuration C.

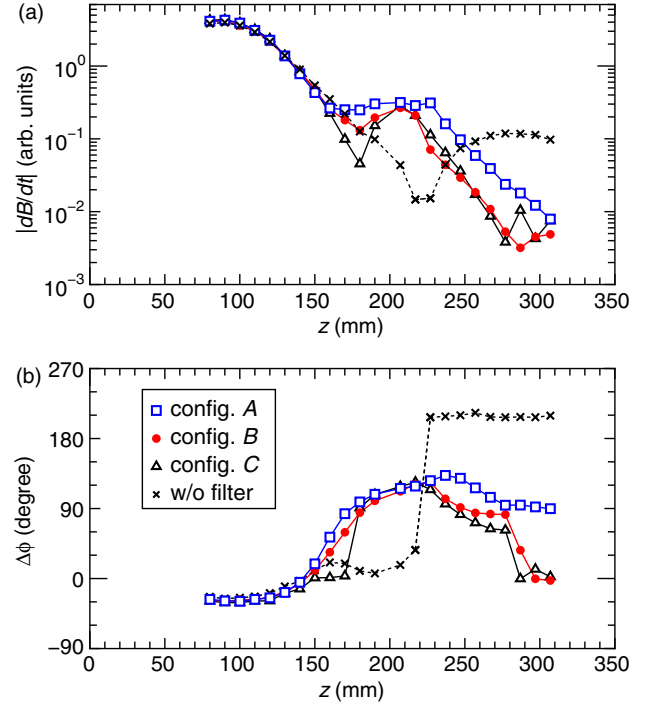


FIG. 3. Axial profiles of (a) the amplitude of the B -dot probe signal $|dB/dt|$ and (b) the phase difference with respect to the rf antenna current.

Furthermore, $\Delta\phi$ at $z \sim 175$ – 225 mm is found to be fairly constant for configurations A–C. These two data imply the presence of the standing wave at $z \sim 175$ – 225 mm. The standing-wave region is found to be shifted upstream when moving the axial location of the MF to the upstream side, as well as the electron heating region in Fig. 2. This shows that the standing-wave structure originates from the presence of the MF. Since the standing-wave region corresponds to the localized high temperature region ($z \sim 220$ mm), the localized electron heating and the resultant ionization can be concluded to be due to the presence of the standing wave. With no MF, on the other hand, the standing-wave structure is seen at $z > 220$ mm, which seems to be due to the axial metallic boundary of the beam extraction grids located at $z = 340$ mm. Based on the above-mentioned wave characteristics, it is discovered that the rapidly bent magnetic field structure plays a role of the axial boundary in the wave propagation, which causes the standing-wave generation.

An axial boundary or rapid change of the refractive index is required to have a standing-wave structure by the wave reflection. To qualitatively discuss the wave reflection by the bent magnetic field, a local refractive index N_z is calculated from a cold dispersion relation with the given magnetic field structure and the measured plasma density, where the wave number is assumed to be in the z direction. The dispersion relation is

$$AN_z^4 - BN_z^2 + C = 0, \quad (1)$$

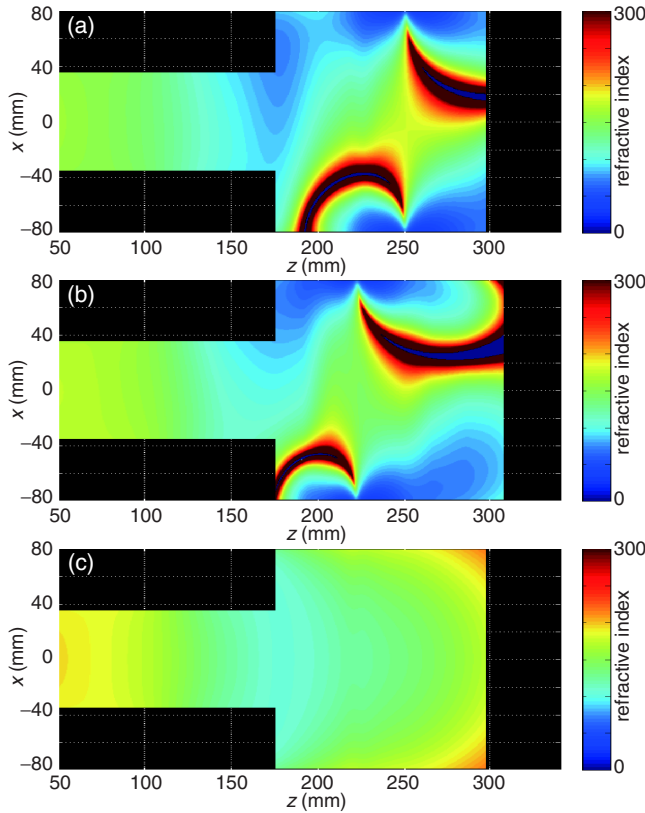


FIG. 4. x - z profiles of the refractive index N_z for cases (a) of configuration A, (b) of configuration C, and (c) with no magnetic filter, where the measured density profile in Fig. 2(d) and the calculated magnetic field vector are used for the calculation.

where A , B , and C are expressed as

$$A = (S \sin^2 \theta + P \cos^2 \theta),$$

$$B = RL \sin^2 \theta + PS(1 + \cos^2 \theta),$$

$$C = PRL,$$

$$R = S + D, L = S - D,$$

with the elements of the dielectric tensor (S , D , P) including both the electron and ion terms [17,36]. θ is the angle between the z axis and the local magnetic field vector. The x profile of the plasma density is assumed to be uniform for further simplicity in discussing the essential physics.

Figure 4 shows the x - z profiles of the calculated N_z for configurations A and C, and with no MF. As seen in Figs. 4(a) and 4(b), the rapid change of N_z is formed around the MF, and the axial location of the rapid change of N_z follows the location of the MF. This rapid change of N_z is not seen for the case with no MF, as in Fig. 4(c). More addressing Figs. 4(a) and 4(b), the large value of N_z near the MF region corresponds to the lower hybrid resonance. However, the wave behaviors near the resonance layer, such as the large wave number, have not been observed here. Since all of the regions—the high density region, the localized electron heating region, the high density region,

the standing wave region, and the region of the rapid refractive index change—follows the location of the MF, it can be deduced again that the wave is reflected by the local change of N_z and the resultant generated standing helicon wave heats the electrons efficiently, unlike the heating at the resonance layer.

It should be mentioned that the measured rf magnetic field is the superimposition of the inductive antenna and wave fields. The larger amplitude inductive field at $z < 175$ mm does not give efficient electron heating, while the downstream standing wave yields the high energy electrons. Although the helicon-wave heating is considered to generate the energetic electrons via some heating processes, e.g., in Refs. [20,37], the detailed heating mechanism by the standing helicon wave is still unclear and demands further study. Moreover, the present configuration seems to behave like a wave resonator by the presence of the rapid change of N_z . The simple wave theory used here cannot well describe the wave field due to the boundary conditions and the non-WKB behavior near the MF. Therefore, more detailed numerical analysis, such as a finite-difference time-domain method and a two- or three-dimensional measurement, is required to achieve further understanding.

Because of the above-mentioned wave reflection by the MF, the decay of the wave amplitude within the MF occurs as seen at $z > 250$ mm in Fig. 3(a), which can prevent the electrons from being heated near the beam extraction grids. Actually, the electron cooling within the MF is also observed in Fig. 2. Hence, the present experiment simultaneously demonstrates the electron heating and the resultant ionization upstream of the MF, and cooling within the MF.

In summary, the rapid change of the refractive index for the rf wave is introduced into the helicon plasma source by using the MF. The wave is reflected due to the presence of the local (nearly discontinuous) change of the refractive index, which is induced not by the physical boundary but by the rapidly bent magnetic field. The resultant standing helicon wave is observed and the electrons are heated by the standing wave. The wave reflection induced by the local change of the refractive index yields the absence of the rf field within the MF; hence, a low electron temperature is obtained there. These features seem to be the inherent and novel characteristics in helicon plasmas which have a nonuniform magnetic field structure.

This work is partially supported by grants-in-aid for scientific research (Grants No. B25287150 and No. A26247096) from the JSPS and LHD Project Collaboration Research (KOAR018), the Yazaki Memorial Foundation for Science, and Technology, and the Casio Science Promotion Foundation.

*kazunori@ecei.tohoku.ac.jp

[1] R. W. Boswell, *Phys. Lett. A* **33A**, 457 (1970).

- [2] R. W. Boswell and F. F. Chen, *IEEE Trans. Plasma Sci.* **25**, 1229 (1997), and references therein.
- [3] F. F. Chen and R. W. Boswell, *IEEE Trans. Plasma Sci.* **25**, 1245 (1997), and references therein.
- [4] A. W. Degeling, C. O. Jung, R. W. Boswell, and A. R. Ellingboe, *Phys. Plasmas* **3**, 2788 (1996).
- [5] K. P. Shamrai and S. Shinohara, *Phys. Plasmas* **8**, 4659 (2001).
- [6] F. F. Chen, *Phys. Plasmas* **10**, 2586 (2003).
- [7] Y. Sakawa, H. Kunitatsu, H. Kikuchi, Y. Fukui, and T. Shoji, *Phys. Plasmas* **11**, 286 (2004).
- [8] V. F. Virko, K. P. Shamrai, Yu. V. Virko, and G. S. Kirichenko, *Phys. Plasmas* **11**, 3888 (2004).
- [9] A. W. Degeling, G. G. Borg, and R. W. Boswell, *Phys. Plasmas* **11**, 2144 (2004).
- [10] Ph. Guittienne, A. A. Howling, and Ch. Hollenstein, *Phys. Rev. Lett.* **111**, 125005 (2013).
- [11] R. L. Stenzel and J. M. Urrutia, *Phys. Rev. Lett.* **114**, 205005 (2015).
- [12] R. W. Boswell, *Plasma Phys. Controlled Fusion* **26**, 1147 (1984).
- [13] M. Nisoo, Y. Sakawa, and T. Shoji, *Jpn. J. Appl. Phys.* **38**, L777 (1999).
- [14] T. Motomura, S. Shinohara, T. Tanikawa, and K. P. Shamrai, *Phys. Plasmas* **19**, 043504 (2012).
- [15] K. Takahashi, A. Chiba, and A. Ando, *Plasma Sources Sci. Technol.* **23**, 064005 (2014).
- [16] O. Grulke, A. Stark, T. Windisch, J. Zalach, and T. Klinger, *Contrib. Plasma Phys.* **47**, 183 (2007).
- [17] D. G. Swanson, *Plasma Waves*, 2nd ed. (Institute of Physics, Bristol, England, 2003).
- [18] H. P. Laqua, V. Erckmann, H. J. Hartfuss, and H. Laqua, *Phys. Rev. Lett.* **78**, 3467 (1997).
- [19] R. L. Stenzel, A. Y. Wong, and H. C. Kim, *Phys. Rev. Lett.* **32**, 654 (1974).
- [20] K. P. Shamrai, V. P. Pavlenko, and V. B. Taranov, *Plasma Phys. Controlled Fusion* **39**, 505 (1997).
- [21] S. John, *Phys. Rev. Lett.* **58**, 2486 (1987).
- [22] E. Yablonovitch, *Phys. Rev. Lett.* **58**, 2059 (1987).
- [23] O. Sakai, T. Naito, and K. Tachibana, *Phys. Plasmas* **17**, 057102 (2010).
- [24] C. Charles, R. W. Boswell, and R. Hawkins, *Phys. Rev. Lett.* **103**, 095001 (2009).
- [25] U. Fantz, P. Franzen, W. Kraus, M. Berger, S. Christ-Koch, M. Fröschle, R. Gutser, B. Heinemann, C. Martens, P. McNeely, R. Riedl, E. Speth, and D. Wunderlich, *Plasma Phys. Controlled Fusion* **49**, B563 (2007).
- [26] A. Aanesland, J. Bredin, P. Chabert, and V. Godyak, *Appl. Phys. Lett.* **100**, 044102 (2012).
- [27] Y. Takeiri, O. Kaneko, K. Tsumori, Y. Oka, K. Ikeda, M. Osakabe, K. Nagaoka, E. Asano, T. Kondo, M. Sato, and M. Shibuya, *Nucl. Fusion* **46**, S199 (2006).
- [28] P. Franzen, H. D. Falter, U. Fantz, W. Kraus, M. Berger, S. Christ-Koch, M. Fröschle, R. Gutser, B. Heinemann, S. Hilbert, S. Leyer, C. Martens, P. McNeely, R. Riedl, E. Speth, and D. Wunderlich, *Nucl. Fusion* **47**, 264 (2007).
- [29] R. S. Hemsworth, A. Tanga, and V. Antoni, *Rev. Sci. Instrum.* **79**, 02C109 (2008).
- [30] M. L. Yu, *Phys. Rev. Lett.* **40**, 574 (1978).
- [31] M. Bacal and M. Wada, *Applied Physics Reviews* **2**, 021305 (2015), and references therein.
- [32] K. N. Leung, K. W. Ehlers, and M. Bacal, *Rev. Sci. Instrum.* **54**, 56 (1983).
- [33] A. Ando, A. Komuro, T. Matsuno, K. Tsumori, and Y. Takeiri, *Rev. Sci. Instrum.* **81**, 02B107 (2010).
- [34] J. Santoso, R. Manoharan, S. O'Byrne, and C. S. Corr, *Phys. Plasmas* **22**, 093513 (2015).
- [35] K. Takahashi, C. Charles, R. W. Boswell, and T. Fujiwara, *Phys. Rev. Lett.* **107**, 035002 (2011).
- [36] T. H. Stix, *Waves in Plasmas* (Springer, New York, 1992).
- [37] R. T. S. Chen and N. Hershkowitz, *Phys. Rev. Lett.* **80**, 4677 (1998).